

Highly sensitive and multispectral responsive phototransistor using tungsten-doped VO₂ nanowires

Cite this: DOI: 10.1039/c4nr00898g

Junpeng Lu,^{†a} Hongwei Liu,^{†b} Suzi Deng,^a Minrui Zheng,^a Yinghui Wang,^a Jeroen A. van Kan,^a Sing Hai Tang,^a Xinhai Zhang,^{*c} Chong Haur Sow^{*a} and Subodh G. Mhaisalkar^d

In this work, we report a novel and feasible strategy for the practical applications of one-dimensional ultrasensitive phototransistors made of tungsten-doped VO₂ single nanowires. The photoconductive response of the single nanowire device was investigated under different visible light excitations (405 nm, 532 nm, and 660 nm). The phototransistor device exhibited ultrafast photoresponse, high responsivity, broad multispectral response, and rapid saturation characteristic curves. These promising results help to promote the applications of this material in nano-scale optoelectronic devices such as efficient multispectral phototransistors and optical switches.

Received 18th February 2014
Accepted 15th April 2014

DOI: 10.1039/c4nr00898g

www.rsc.org/nanoscale

Introduction

Photoconductions in nanowires have attracted widespread attention due to their unique properties that contribute to the high photosensitivity of such nanostructures.^{1–6} Firstly, the large surface to volume ratio and the existence of surface trap states in nanowires could greatly prolong the photocarrier lifetime. In addition, the reduced size of the active working region in nanowire devices shortens the carrier transit time. Indeed, the concurrence of the long lifetime and short transit time of photocarriers will facilitate substantial photoconductive gain.^{7–8} These promising properties result in the applications of semiconductor nanowires as photodetectors, photovoltaics, optical switches, and optical interconnects.^{9–13} Among these applications, a phototransistor is an attractive device as it is one of the basic building blocks for nano-optoelectronic circuits. In the last decade, extensive research effort has been devoted to such a device due to its significantly lower noise and higher sensitivity than those of its counterparts.^{14,15} However, reported phototransistors have faced challenges such as slow response rate^{16–18} or excessively high working voltage (>10 V),^{19–21} restraining the performance of optoelectronic devices. Furthermore, the

saturation of the output current is not easy to achieve, which limits the rectification application of transistors.^{16,22} Among the metal oxide nanowires, vanadium dioxide (VO₂) nanowires have attracted great attention.^{23,24} Research interests on this nanostructure focus on its metal–insulator transition and related properties.^{25–27} However, little attention has been paid to the optoelectronic applications of VO₂ due to its low photoresponse at room temperature, whilst its low n-type electrical conductivity always restricts its practical applications. Impurity doping is one of the most commonly employed techniques for modifying the electrical properties of a material. Recently, the use of substitutional doping of both vanadium and oxygen sublattices has been extensively explored to appreciably reduce the phase transition temperature.^{28,29} Substituting vanadium with tungsten is particularly attractive and results in a depression in the phase transition in vanadium oxide.^{30,31} Most recently, W-doped VO₂ one-dimensional (1D) nanostructure was synthesized and its phase transition property was shown to be influenced by the combination of doping and finite size.³² However, the optoelectronic properties of such W-doped VO₂ nanostructures and their corresponding applications have still not been studied. In this work, we present a comprehensive study on the optoelectronic properties of W-doped VO₂ nanowires. The work begins with the solution synthesis of tungsten-doped VO₂ nanowires by a facile hydrothermal approach. Upon the substitution of vanadium with tungsten, the electron donor levels become extremely shallow, facilitating a supersensitive phototransistive process and yielding an ultrafast photocurrent response along with a broad multispectral response. In addition, the saturation of the light intensity gated output current could be easily achieved within the bias of 1.5 V. We analyzed the charge transport under laser irradiation with different wavelengths and a series

^aDepartment of Physics, National University of Singapore, 2 Science Drive 3, 117542, Singapore. E-mail: physowch@nus.edu.sg

^bInstitute of Materials Research and Engineering, A*STAR (Agency for Science, Technology and Research), 3 Research Link, 117602, Singapore

^cDepartment of Electrical and Electronic Engineering, South University of Science and Technology of China, 1088 Xueyuan Road, Xili, Nanshan District, Shenzhen, Guangdong, China 518055. E-mail: zhang.xh@sustc.edu.cn

^dSchool of Materials Science and Engineering, Nanyang Technological University, Blk N4.1, Nanyang Avenue, 639798, Singapore

[†] These authors have made equal contribution to this work.

of light intensities. We found that the device could be controlled readily. These results demonstrate the promising potential of tungsten-doped VO₂ nanowires in nano-scaled optoelectronic applications.

Experimental section

A simple and template-free hydrothermal method was employed for the synthesis of tungsten-doped VO₂ nanowires.³³ Briefly, 0.5 g of V₂O₅ powder was dispersed in 40 mL of deionized water ($\rho = 18.2 \text{ M}\Omega \text{ cm}^{-1}$) under vigorous stirring. Subsequently, 0.6 g of H₂C₂O₄ (oxalic acid) mixed with 0.03 g of H₂WO₄ (tungstic acid) was slowly added into this dispersion. After stirring for 3 hours to yield a bright orange suspension, the resulting mixture was transferred into a 50 mL Teflon container and then sealed in an autoclave using a high-pressure Parr acid digestion bomb. The autoclave was kept in an oven and the system temperature was increased to 250 °C and maintained for 72 h. After cooling to room temperature, dark blue precipitates were collected. The product was washed with acetone solution and deionized water several times, and then dried overnight in vacuum at 70 °C.

After the synthesis, a single W-doped VO₂ nanowire was transferred to a silicon substrate coated with a 200 nm thick Si₃N₄ dielectric layer for device fabrication and subsequent electronic characterization. A UV laser lithography system (Heidelberg Instruments μ PG101) was used to fabricate the device. The device fabrication was completed by thermal evaporation of 20 nm cobalt and 280 nm gold as the source-drain electrodes.

The single nanowire phototransistor characterization was carried out by irradiating the nanowire with a laser beam bigger than the size of the nanowire in a high vacuum chamber. For determination of the carrier lifetime, a focused laser beam from a diode laser in conjunction with a modified optical microscope was employed. The focused laser beam system was a home-built scanning photocurrent microscopy (SPCM) unit. SPCM is an ideal technique for probing various physical properties of 1D nanostructures, such as local band bending, barrier heights, electrical field distribution, and carrier diffusion lengths.^{34–40} Our SPCM set-up involves irradiating a focused laser spot (<1 μm) on a selected position of a planar device while recording the photocurrent as a function of the focused laser spot, *i.e.*, local photocarrier injection position. The measurements were carried out by utilizing Keithley 6430 sourcemeter under a constant bias. A heating stage (Linkam Scientific Instruments, TMS 94) was employed for the thermal cycling experiments.

Results and discussions

The morphology of the as-synthesized products was characterized by scanning electron microscopy (SEM). A typical SEM image of the nanowires is shown in Fig. 1a. The nanowires exhibit rectangular cross-sections with smooth and well faceted surfaces. The typical size of the cross-section of the as-synthesized nanowires is in the range of 300–800 nm and the length is

in the range of 5–30 μm . The XRD pattern recorded from the nanowires drop-casted on a Si substrate is shown in Fig. 1b. The peaks obtained can be indexed to the stable monoclinic VO₂ (M1) polymorph. We do not see any signals for the formation of metastable VO₂ (B) polymorph due to the high temperature environment during the synthesis.³² As compared with undoped VO₂, the interplanar spacing increases after substitutional W incorporation. This is consistent with the larger atomic radius of the dopant W⁶⁺ ion³³ and the possible existence of the M2 phase.⁴¹ Further structural characterization of the nanowires was carried out by micro-Raman spectroscopy. Fig. 1c depicts the room temperature Raman spectrum of W-doped VO₂ nanowires. The space groups for M1 and M2 lattices are C_{2h}^3 and C_{2h}^5 , respectively.⁴² Therefore, the M1 phase is characterized by 18 Raman-active modes, namely, 9A_g and 9B_g modes, as per the group theory.⁴³ The M2 phase also has 18 Raman active modes with a slightly different distribution, namely, 10A_g and 8B_g modes, due to the pronounced differences in the local symmetry.⁴⁴ The Raman spectrum shown in Fig. 1c is consistent with previously reported Raman studies and group theory predictions,^{45–47} despite the small shifts in the A_g modes from 607 and 189 cm^{-1} to 620 and 196 cm^{-1} , respectively. These shifts are probably due to the tungsten doping³³ or the existence of the M2 phase resulting from the incorporation of the substitutional W dopant.⁴¹ Transmission electron microscopy (TEM) was employed to investigate the crystalline lattice of the W-doped VO₂ nanowires. Fig. 1d illustrates the low-magnification TEM image of a single nanowire, the corresponding selected area electron diffraction (SAED) and high-resolution TEM (HRTEM) image. The fringe spacings between adjacent lattice planes are measured to be 2.433 Å and 2.427 Å, corresponding to the (020) and (211) interplanar distances, respectively.

Fig. 2a illustrates the schematic architecture of the fabricated single nanowire phototransistor device and the corresponding SEM image of the device; two finger electrodes are shown in the inset of Fig. 2b. The separation between the two electrodes is 15 μm . Energy-dispersive spectroscopy (EDX) was carried out on randomly selected spots along the nanowire, and the representative spectrum is shown in Fig. 2b. The tungsten peak is clearly demonstrated, which indicates that the W atoms have been doped into VO₂ successfully. We denote the W-doped VO₂ nanowire as W_xV_{1-x}O₂, where *x* denotes the atomic ratio of W as a fraction of the substituted vanadium sublattice. As revealed by the EDX spectrum, the utilized VO₂ nanowire is doped with about 0.42 at% W. Since the metal-insulator transition is a notable feature of VO₂,^{48,49} we measured the temperature dependent electrical resistance from a single W_xV_{1-x}O₂ nanowire device. As shown in Fig. 2c, with increasing temperature, the two-terminal resistance steadily decreases, exhibiting the classical activated semiconductor transport property, and switches over to metallic behavior for temperatures above 50 °C. Upon cooling, the nanowire displays a reverse jump to the insulating phase at a lower temperature of 27 °C, thus a pronounced hysteresis is exhibited. The phase transition temperature is significantly lower than pure VO₂ nanowires (67 °C), which is due to the increased free carrier density with W doping. This result is

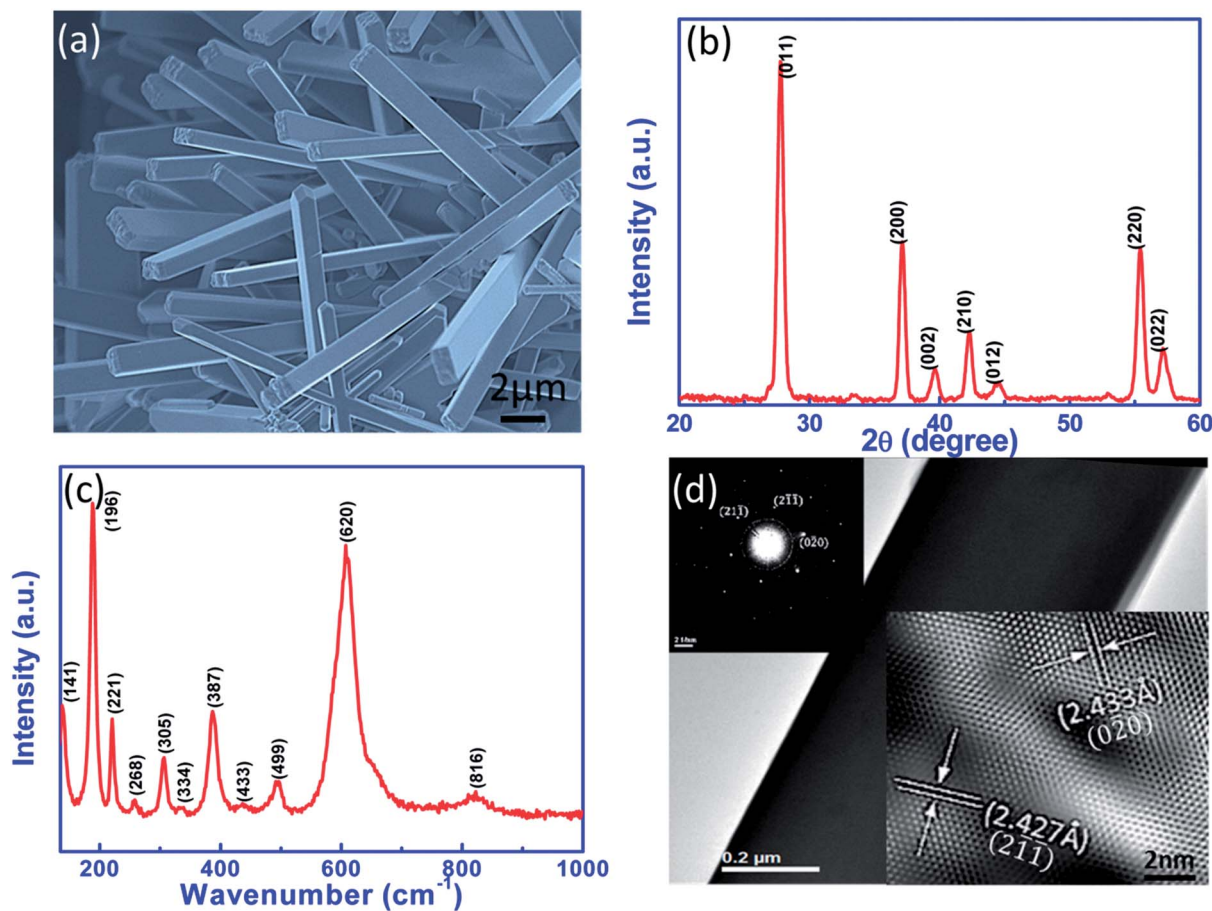


Fig. 1 (a) SEM image of the as-synthesized nanowires. (b) XRD pattern of the nanowires indicates a stable monoclinic polymorph. (c) Raman spectrum of the nanowires. (d) Low-magnification TEM image of a single nanowire. Inserts show the SAED and HRTEM of the nanowire.

consistent with the behavior of $W_xV_{1-x}O_2$ nanobelts reported by Banerjee and co-workers.³²

Fig. 2d shows the typical I - V curves of the nanowire device in dark condition and under a 532 nm broad laser beam illumination with light intensities of 25 mW cm^{-2} and 50 mW cm^{-2} , respectively. The voltage was swept from 0 to 4 V, and all the measurements were carried out at room temperature. Due to the higher work function of the metal electrodes, the metal-semiconductor junction resulted in the formation of a Schottky barrier between the nanowire and the Au electrodes.⁵⁰ The I - V behavior under 532 nm laser illumination drastically differs from the dark I - V behavior. The I - V characteristics under illumination exhibit an obvious non-linear behavior. The output current increases sharply from 0 V and subsequently reaches near saturation at 1.5 V for 25 mW cm^{-2} illumination (2 V for the 50 mW cm^{-2} case). A change in magnitude of about $50 \mu\text{A}$ is observed in this case. The rapid increase and saturation of the photocurrent suggests the potential of $W_xV_{1-x}O_2$ nanowire as an ultrasensitive phototransistor. The dark I - V behavior indicates that the nanowire was highly resistive, while under laser light irradiation (laser wavelength = 532 nm; photon energy = 2.33 eV), the conductance of the nanowire increases significantly. We preliminarily ascribe this dramatic increase to the

photogenerated free carriers rather than the light induced phase transition since the laser intensity was carefully controlled well below the phase transition threshold of VO_2 , which is about 20 kW cm^{-2} at room temperature.⁵¹ Even though the threshold of laser induced phase transition for $W_xV_{1-x}O_2$ nanowire would be lower than that of VO_2 , the power intensity of several tens of mW cm^{-2} is much lower than the expected phase transition threshold of $W_xV_{1-x}O_2$ nanowire. To further support this claim, finite element method (FEM) was employed to simulate the temperature increase caused by the laser irradiation. The result indicates that the local temperature increased from room temperature (298 K) to 304 K at a light intensity of 100 mW cm^{-2} , as shown in Fig. 2e. This value is much lower than the phase transition temperature.

The output characteristics under the illumination of a series of intensities of 532 nm laser light are shown in Fig. 3a. With the increase of incident light power intensity, the output current rises gradually. Evidently, the output current is controlled by the light power intensity, and the output curves display good transistor behavior, consisting of a rapidly increasing linear regime and a fully saturated regime, which is similar to the output characteristics of a traditional field effect transistor controlled by gate voltage, except the light intensity plays the role of voltage

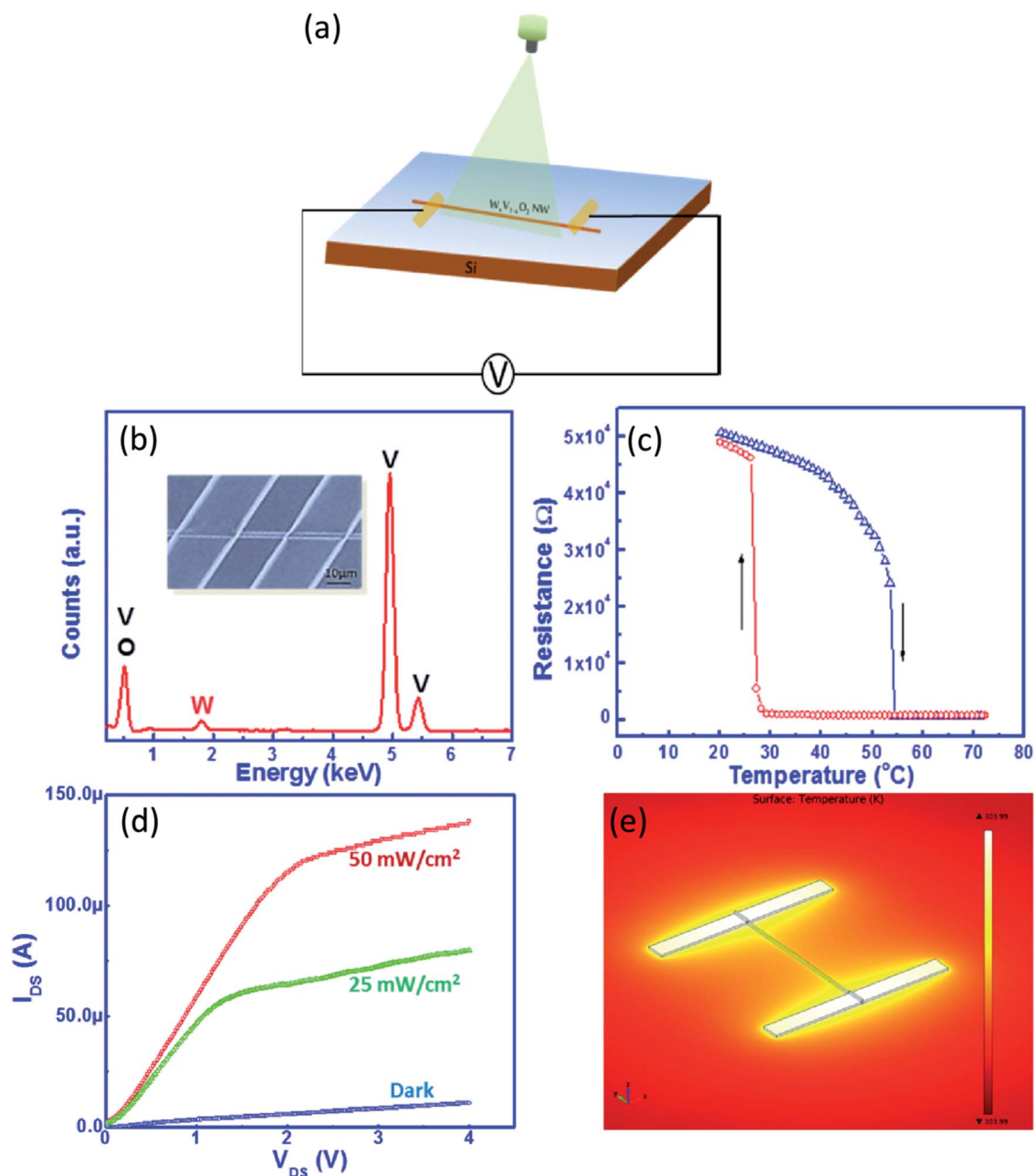


Fig. 2 (a) Schematic of a single nanowire device and the broad beam laser setup. (b) EDX spectrum of the single nanowire indicates the tungsten doping. Inset shows the SEM image of the nanowire device. (c) Demonstration of the metal–insulator transition property of the $W_xV_{1-x}O_2$ nanowire. (d) I – V curves of the device in dark and under 532 nm laser illumination at intensities of 25 mW cm^{-2} and 50 mW cm^{-2} . (e) Simulation result of the temperature distribution on the nanowire device.

gating in this case. The results suggest that the incident light could be employed to replace the gate voltage, V_{GS} , as an additional terminal to control the output current of the transistor, indicating an effective approach to achieve current modification and signal magnification in a single nanowire device for future low-cost, nanoscale photoelectric integration. As described above, the $W_xV_{1-x}O_2$ nanowire phototransistors are expected to show the photoresponse to multispectral light. Fig. 3b and c show the output characteristics of the nanowire device under different intensities of 405 nm and 660 nm light irradiation,

respectively. Similar phototransistor behavior is observed as that under 532 nm light illumination. The output current can also be well controlled by the incident light intensity and saturation is achieved at higher voltages, indicating the wide application potential, easy realizability and flexible maneuverability of the $W_xV_{1-x}O_2$ nanowire phototransistors. Fig. 3d shows the variation of photocurrent ($I = I_{\text{photo}} - I_{\text{dark}}$) measured at the bias of 4 V with light intensity. The photocurrent *versus* illumination light intensity can be described by a power law dependence in the form of $I = AP^\alpha$,^{52,53} where I is the

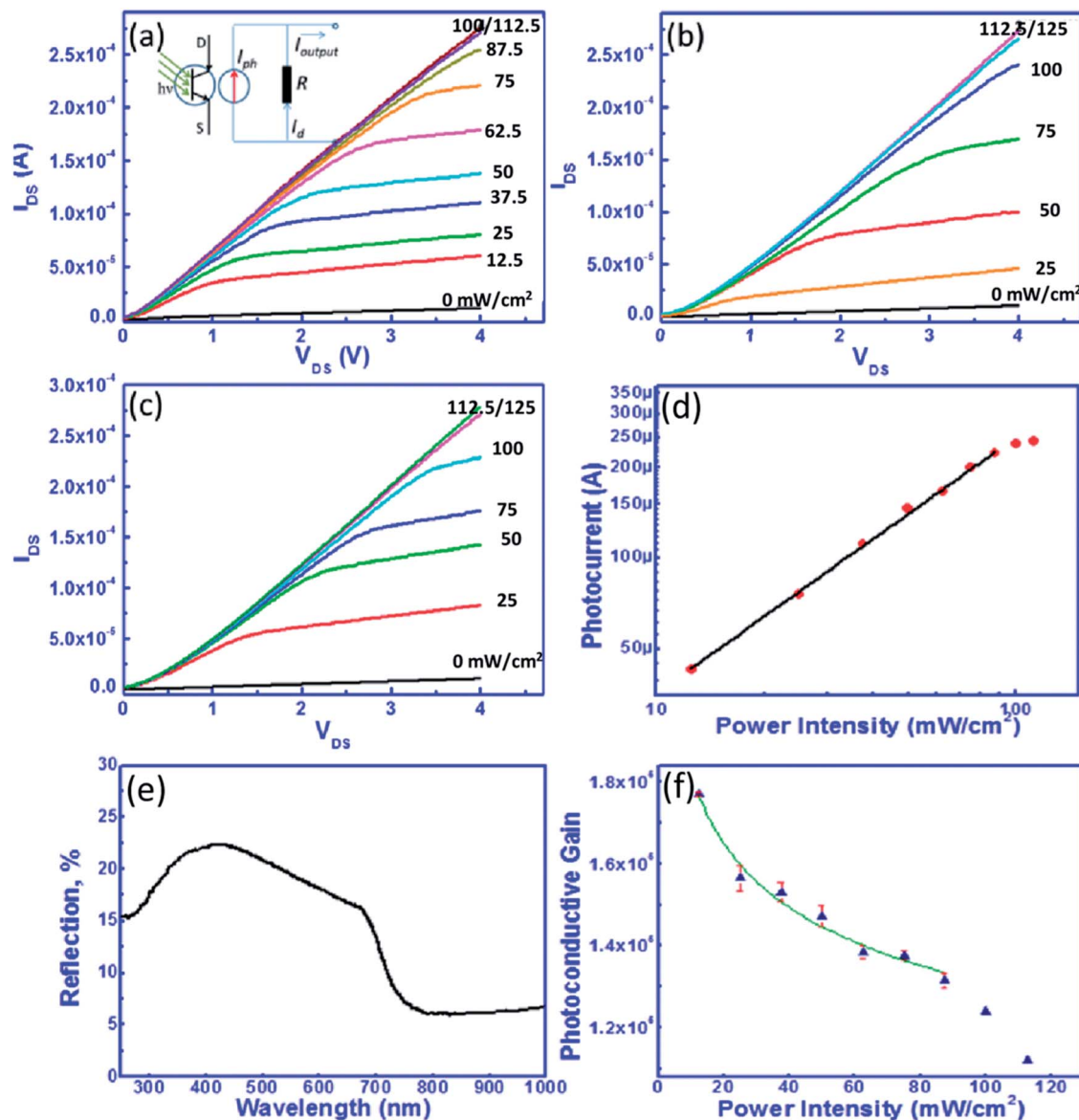


Fig. 3 Output characteristics curves of the device under (a) 532 nm, (b) 405 nm, and (c) 660 nm light illumination at different intensities. (d) Photocurrent versus intensity plot at bias of 4 V. (e) Reflection spectrum of as-synthesized nanowires. (f) Photoconductive gain versus intensity plot at bias of 4 V.

photocurrent, A is a proportionality constant, P is the power intensity and the exponent α is an empirical value (usually smaller than unity).^{8,54} As displayed in Fig. 3d, the photocurrent versus light intensity variation at a bias of 4 V is well fitted with the power law as $I \sim P^{0.82}$ when the light intensity is lower than 100 mW cm^{-2} . The high α value indicates the strong dependence of the photocurrent on light intensity. When there is a uniform distribution of trap states, the photocurrent dependence on the incident light intensity would be linear; consistent with this, the photogeneration efficiency of the charge carrier is proportional to the absorbed photon flux.^{7,55} The non-integer power dependence of the $\text{W}_x\text{V}_{1-x}\text{O}_2$ nanowire device could be attributed to a complex process of carrier generation, recombination and trapping along the nanowire.¹⁰ However, further

increasing the incident power intensity leads to the photocurrent saturation at higher light intensities (beyond 100 mW cm^{-2}). Bube first demonstrated the saturation of photocurrent with light intensity in CdS crystals in 1960.⁵⁶ The occurrence of saturation was interpreted as resulting from the saturation of sensitizing energy levels in the crystal. Namely, the centers with a large cross section for holes and a subsequent small cross section for electrons were completely occupied by holes. Additional excited holes generated by further increasing the light intensity could be captured only at the centers with large cross sections for electrons. Thus, the saturated photocurrent was considered to be composed of current arising from long lifetime electrons with density equal to that of the sensitizing band and short lifetime electrons produced by the absorption of photons

over and above those needed to saturate the sensitizing centers. Mueller and co-workers also observed similar photocurrent saturation in graphene photodetectors.⁵⁷ This phenomenon was attributed to the screening effect as observed in conventional photodiodes. In the case of nanowires, the photocurrent saturation at high light intensity can be attributed to the carrier-trap saturation effect.⁷ At high light intensity, the density of available carrier-traps in the nanowire is cumulatively reduced, resulting in the saturation of the photoresponse. Photoconductivity in semiconducting metal oxide nanowires (such as ZnO) can be attributed to the increased charge carriers by exciting the electrons to the conduction band and the oxygen adsorption-desorption process on the nanowire surface.^{7,58,59} In $W_xV_{1-x}O_2$ nanowires, the photoconductivity can originate from the excitation from the mid gap electronic state introduced by W doping. This mid gap band can be assigned as a donor type photoionization of the tungsten dopant, which generates delocalized charge carriers upon photoexcitation. Fig. 3e shows the reflection spectrum of these nanowires, and the spectrum indicates that the nanowires show absorption ranging from the UV to IR range. Therefore, the $W_xV_{1-x}O_2$ nanowire is anticipated to show photoresponse to multispectral light from UV to NIR. Light from this band can generate mobile charge carriers thereby increasing the charge carrier density, inducing photocurrent in the nanowires. The other mechanism is oxygen adsorption-desorption in which upon excitation of the nanowire with photons, the oxygen adsorbed on the nanowire surface is desorbed, releasing the surface bound electrons in the depletion layer, and hence, increasing the conductance of the nanowire. The oxygen adsorption-desorption effect in this experiment can be considered to be minimal, since we carried out the characterization in high vacuum.

Various photoconductive parameters such as responsivity, external quantum efficiency, photoconductive gain, photocurrent rise time and decay time, and stability of the photocurrent are analyzed to evaluate the performance of a nanowire device as a phototransistor. The phototransistor's responsivity (R_{res}) is defined as the photocurrent per unit power on the effective area of the phototransistor and can be calculated by⁶⁰

$$R_{\text{res}} = \frac{I_{\text{pho}}}{P_{\text{opt}}} = \frac{(I_{\text{illum}} - I_{\text{dark}})S^{-1}}{P_{\text{inc}}} \quad (1)$$

where I_{pho} is the photocurrent and P_{opt} is the light power. I_{illum} and I_{dark} are the output current under illumination and in dark, respectively, S is the effective area of the nanowire device, and P_{inc} is the power density. It is very attractive that the R_{res} value of the $W_xV_{1-x}O_2$ nanowire phototransistor could reach as high as $(2.15 \pm 0.2) \times 10^7 \text{ mA W}^{-1}$ at a light intensity of 50 mW cm^{-2} at 4 V bias. This R_{res} value is much higher than that of graphene ($\sim 1 \text{ mA W}^{-1}$),⁶¹ MoS_2 (7.5 mA W^{-1}),²² and organic (PPEs, 36 mA W^{-1})¹⁷ phototransistors. It is even higher than those of ZnO nanowires ($1.29 \times 10^7 \text{ mA W}^{-1}$)¹⁸ and recently reported K_xMoO_3 nanowire phototransistors ($1.75 \times 10^7 \text{ mA W}^{-1}$)⁶² and comparable with vertically aligned Si nanowire arrays ($\sim 10^8 \text{ mA W}^{-1}$).⁶³ The high responsivity of the nanowire device enables a large on/off ratio, indicating the potential applications of the nanowire phototransistor in optoelectronic devices such as

optoisolators, retrosensors,^{16,64} and photoamplifiers. The related diagram and equivalent circuit of the $W_xV_{1-x}O_2$ nanowire transistor are illustrated in the inset of Fig. 3a, where R is the intrinsic resistance of the $W_xV_{1-x}O_2$ nanowire.

The photoconductivity enhancement is quantitatively analyzed by calculating the photoconductive gain, which is a critical parameter for evaluating the sensitivity of phototransistors. The photoconductive gain is defined as the ratio between the number of collected electrons per unit time and the number of absorbed photons per unit time, and can be expressed for simplicity as⁵²

$$G = \frac{N_{\text{ele}}}{N_{\text{pho}}} = \frac{I_{\text{pho}}}{P_{\text{abs}}} \times \frac{h\nu}{e} \quad (2)$$

where P_{abs} is the light power absorbed by the effective working area, and $h\nu$ is the energy of an incident photon. Fig. 3f shows the calculated photoconductive gain *versus* various light intensities at 4 V bias. Here, the light power absorbed by the nanowire is lesser than the incident power. When a laser light is incident onto the interface of two materials with different refractive indices (n_1, n_2), Fresnel reflection occurs. When the incident light is perpendicular to the interface, the transmission rate can be calculated by $4n_1n_2/(n_1 + n_2)^2$.⁵⁴ Taking into account the Fresnel reflection from the nanowire, the photoconductive gain can be calculated and the gain decreases with increasing light intensity. Similar to the increasing photocurrent with light intensity, at lower light intensity ($<100 \text{ mW cm}^{-2}$), the relationship between the photoconductive gain and the light intensity can be described with an inverse power law with a fractional power dependence of the gain in $W_xV_{1-x}O_2$ nanowires ($G \sim P^{-1.5}$). At higher light intensity, the photoconductive gain deviates below this power law dependence. The decreasing photoconductive gain results mainly from the carrier trap saturation effect. Under such a saturation condition, the photoconductive gain can also be derived and expressed for simplicity as⁷

$$G = \frac{I_{\text{pho}}}{eF} = \left(\frac{T_1}{T_t}\right) \frac{1}{1 + (F/F_0)^n} \quad (3)$$

where F is the photon absorption rate, F_0 is the absorption rate when trap saturation occurs, T_1 is the carrier lifetime, and T_t is the carrier transit time. The first term on the right-hand side is the usual description for the photoconductive gain, which is the ratio of carrier lifetime to carrier transit time, whilst the second term describes trap saturation at high excitation intensities. As displayed in Fig. 3f, the extremely long photocarrier lifetime accompanied by the short carrier transit time due to the small dimensionality of the nanowire device facilitates photoconductive gain as high as $G = 1.8 \times 10^5$. The decrease of the gain at relatively high light intensities is a manifestation of trap saturation. In addition to this reason, the onset of carrier recombination at higher light intensities may also contribute to the shortening of the carrier lifetime.^{7,65} To determine the carrier lifetime, an SPCM setup was employed to carry out the line scans rastered over the nanowire device. Fig. 4a schematically illustrates the SPCM setup where a focused micro-size laser spot is scanned along the $W_xV_{1-x}O_2$ nanowire. The

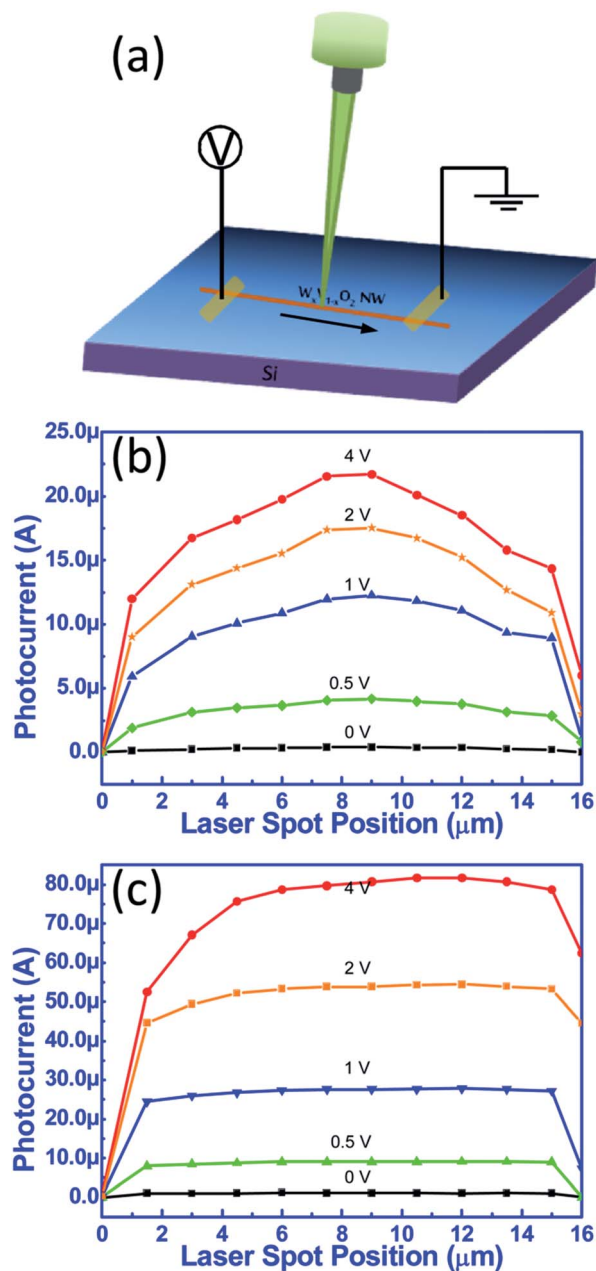


Fig. 4 (a) Schematic of the SPCM setup, where the focused laser spot is rastered over the nanowire device. SPCM line scans at different biases under (b) 10 mW cm^{-2} and (c) 30 mW cm^{-2} light intensities. The asymmetrical plot is due to the formation of Schottky contact between the nanowire and the electrode.

photocurrent profiles under different applied biases ranging from 0 V to 4 V with lower light intensity (10 mW cm^{-2}) and higher light intensity (30 mW cm^{-2}) irradiation are shown in Fig. 4b and c, respectively. Evidently, the most apparent difference in the photocurrent profile under bias with different light intensities is the appearance of higher magnitude around the center of the nanowire in Fig. 4b, whilst the profile is almost flat in Fig. 4c. This observed photocurrent profile under applied bias is an indication that the carrier lifetime at low light intensity is significantly longer than that at higher light

intensity in $\text{W}_x\text{V}_{1-x}\text{O}_2$ nanowires. Yu and co-workers⁶⁶ attributed this feature of the photocurrent profiles to the longer carrier lifetimes in VO_2 nanobelts with similar SPCM results, and supported this feature with the experimental results and a numerical simulation of the electrostatics of free carriers in 1D nanostructures under steady state local illumination, following the method described elsewhere.⁶⁷ For a given 1D system, local irradiation usually generates nonequilibrium carriers with lower densities. If the carriers possessed short lifetimes, the photocurrent profile had a flat line shape with no discernible peak, as shown in Fig. 4c. This is because the nonequilibrium carriers with short lifetimes would not reach the electrodes. However, when the carrier lifetime is long enough, even weak illumination could generate high nonequilibrium carrier densities, since the recombination rate is low enough to allow a high density of carriers to accumulate in the steady state.⁶⁶ In this case, the photocurrent profile under bias develops a broad peak and the peak is located where the real current switches from being dominated by the electron current to being dominated by the hole current.³⁷

The promising phototransistor performance is also supported by the ultrafast photoresponse of $\text{W}_x\text{V}_{1-x}\text{O}_2$ nanowire to light illumination, which determines the capability of the device to follow fast-varying optical signals. The rapid response time was detected by an oscilloscope (DSO-X 3024A, 200 MHz) associated with an electronic chopper (SRS SR540). The experimental setup is schematically illustrated in Fig. 5a. In this setup, the light chopper was employed to turn the laser on and off while the oscilloscope was utilized to monitor the time dependence of the output current. The transient response of the transistor has been investigated under applied bias of 1 V and illumination of different wavelengths of light, namely, 405 nm, 532 nm, and 660 nm. Illumination was switched on and off periodically. As shown in Fig. 5b, the device shows a rapid on/off switching behavior. Each photoresponse cycle consists of three distinct stages: a sharp rise, a steady state, and a sharp decay process to the original state with the amplification ratios, $(I_{\text{pho}} - I_{\text{dark}})/I_{\text{dark}}$, ranging from 1667% to 2300% under 87.5 mW cm^{-2} illumination. The fast photocurrent rise and decay times were estimated from the photocurrent *versus* time plots and shown in Fig. 5c and d, respectively. The rise time is defined as the time needed to reach 90% of the photocurrent from dark current upon laser irradiation, and the decay time is defined as the time needed to decay from the current value to 10% after switching off the light. Accordingly, the rise and decay times were measured as 4.8 ms and 3.9 ms, respectively. These rapid frequencies (0.21 and 0.26 kHz) are much faster than those of the reported organic (F16CuPc, 50 Hz and TA-PPE, 100 Hz) and inorganic (ZnO) phototransistors and photoswitches.^{16–18} It is even slightly faster than the recently reported K_xMoO_3 and TiO_2/C core/shell nanowires.^{62,68} The 3 dB bandwidth ($f_{3\text{dB}}$) of the present device can be calculated to be about 0.73 kHz from the expression $f_{3\text{dB}} = 0.35/t_r$.⁵² This fast response frequency and wide response range demonstrate the promising potential of $\text{W}_x\text{V}_{1-x}\text{O}_2$ nanowires as the building blocks in ultrafast nanophotonic devices.

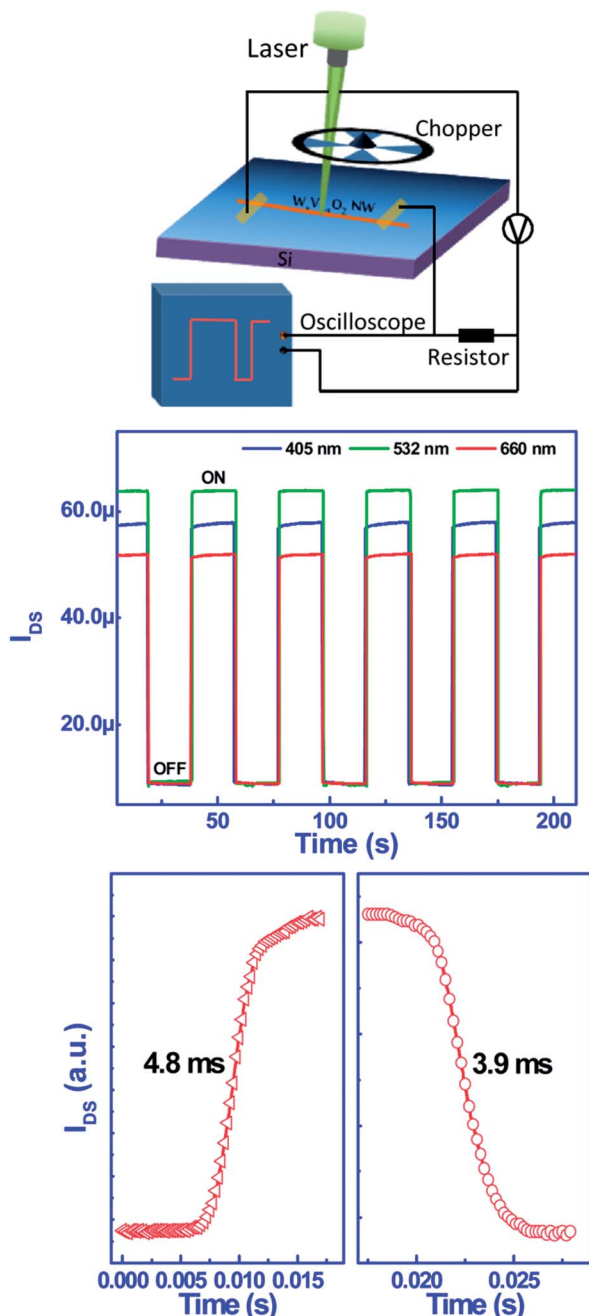


Fig. 5 (a) Schematic diagram of time response measurement setup. (b) Photoresponse characteristics at different wavelengths. (c) and (d) Photoswitching rate test of the device.

Conclusions

In conclusion, a simple, low cost but effective hydrothermal approach was developed and employed to synthesize high quality single crystalline $W_xV_{1-x}O_2$ nanowires with high yield. Based on these nanowires, single nanowire phototransistors were fabricated and systematically characterized. The extreme shallow donor created by the doping of W enables an ultra-sensitive and superfast photocurrent response. The characteristic curves of the device demonstrated that the saturation of the

output current can be achieved within a voltage window of 1.5 V, and light can control the current level, facilitating the application of a single nanowire device as a promising phototransistor and photosensor. Moreover, the high responsivity and broad multispectral response further reveal the potential of this material in nano-optoelectronic applications for sensing, imaging and communications.

Acknowledgements

This work is supported by the Singapore National Research Foundation under CRP Award no. NRF-CRP-4-2008-03. The authors also acknowledge the support from the NUS FRC Grant no. R-144-000-281-112.

Notes and references

- 1 L. Peng, L. Hu and X. Fang, *Adv. Mater.*, 2013, **25**, 5321.
- 2 S.-B. Wang, R.-S. Chen, S. J. Chang, H.-C. Han, M.-S. Hu, K.-H. Chen and L.-C. Chen, *Nanoscale*, 2014, **6**, 1264.
- 3 X. Fang, Y. Bando, M. Liao, U. K. Gautam, C. Zhi, B. Dierre, B. Liu, T. Zhai, T. Sekiguchi, Y. Koide and D. Golberg, *Adv. Mater.*, 2009, **21**, 2034.
- 4 L. Hu, M. M. Brewster, X. Xu, C. Tang, S. Gradečak and X. Fang, *Nano Lett.*, 2013, **13**, 1941.
- 5 X. Fang, S. Xiong, T. Zhai, Y. Bando, M. Liao, U. K. Gautam, Y. Koide, X. Zhang, Y. Qian and D. Golberg, *Adv. Mater.*, 2009, **21**, 5016.
- 6 W. Wang, J. Qi, Q. Wang, Y. Huang, Q. Liao and Y. Zhang, *Nanoscale*, 2013, **5**, 5981.
- 7 C. Soci, A. Zhang, B. Xiang, S. A. Dayeh, D. P. R. Aplin, J. Park, X. Y. Bao, Y. H. Lo and D. Wang, *Nano Lett.*, 2007, **7**, 1003.
- 8 J. S. Jie, W. J. Zhang, Y. Jiang, X. M. Meng, Y. Q. Li and S. T. Lee, *Nano Lett.*, 2006, **6**, 1887.
- 9 C. Soci, A. Zhang, X.-Y. Bao, H. Kim, Y. Lo and D. Wang, *J. Nanosci. Nanotechnol.*, 2010, **10**, 1430.
- 10 H. Kind, H. Yan, B. Messer, M. Law and P. Yang, *Adv. Mater.*, 2002, **14**, 158.
- 11 L. Hu and G. Chen, *Nano Lett.*, 2007, **7**, 3249.
- 12 W. U. Huynh, J. J. Dittmer and A. P. Alivisatos, *Science*, 2002, **295**, 2425.
- 13 B. Tian, T. J. Kempa and C. M. Lieber, *Chem. Soc. Rev.*, 2009, **38**, 16.
- 14 A. J. Seeds and A. A. A. de Salles, *IEEE Trans. Microwave Theory Tech.*, 1990, **38**, 577.
- 15 T. P. I. Saragi, R. Pudzich, T. Fuhrmann and J. Salbeck, *Appl. Phys. Lett.*, 2004, **84**, 2334.
- 16 Q. Tang, L. Li, Y. Song, Y. Liu, H. Li, W. Xu, Y. Liu, W. Hu and D. Zhu, *Adv. Mater.*, 2007, **19**, 2624.
- 17 H. Dong, H. Li, E. Wang, H. Nakashima, K. Torimitsu and W. Hu, *J. Phys. Chem. C*, 2008, **112**, 19690.
- 18 W. Y. Weng, S. J. Chang, C. L. Hsu and T. J. Hsueh, *ACS Appl. Mater. Interfaces*, 2011, **3**, 162.
- 19 T. B. Singh, R. Koeppe, N. S. Sariciftci, M. Morana and C. J. Brabec, *Adv. Funct. Mater.*, 2009, **19**, 789.
- 20 A. Zhang, S. You, C. Soci, Y. Liu, D. Wang and Y.-H. Lo, *Appl. Phys. Lett.*, 2008, **93**, 121110.

- 21 Y. Guo, C. Du, C.-A. Di, J. Zheng, X. Sun, Y. Wen, L. Zhang, W. Wu, G. Yu and Y. Liu, *Appl. Phys. Lett.*, 2009, **94**, 143303.
- 22 Z. Yin, H. Li, H. Li, L. Jiang, Y. Shi, Y. Sun, G. Lu, Q. Zhang, X. Chen and H. Zhang, *ACS Nano*, 2012, **6**, 74.
- 23 B. S. Guiton, Q. Gu, A. L. Prieto, M. S. Gudixsen and H. Park, *J. Am. Chem. Soc.*, 2005, **127**, 498.
- 24 J. I. Sohn, H. J. Joo, A. E. Porter, C.-J. Choi, K. Kim, D. J. Kang and M. E. Welland, *Nano Lett.*, 2007, **7**, 1570.
- 25 J. M. Baik, M. H. Kim, C. Larson, A. M. Wodtke and M. Moskovits, *J. Phys. Chem. C*, 2008, **112**, 13328.
- 26 L. Whittaker, C. Jaye, Z. Fu, D. A. Fischer and S. Banerjee, *J. Am. Chem. Soc.*, 2009, **131**, 8884.
- 27 J. Liu, Q. Li, T. Wang, D. Yu and Y. Li, *Angew. Chem., Int. Ed.*, 2004, **43**, 5048.
- 28 M. Netsianda, P. E. Ngoepe, C. R. A. Catlow and S. M. Woodley, *Chem. Mater.*, 2008, **20**, 1764.
- 29 K. Shibuya, M. Kawasaki and Y. Tokura, *Appl. Phys. Lett.*, 2010, **96**, 022102.
- 30 I. P. Parkin and T. D. Manning, *J. Chem. Educ.*, 2006, **83**, 393.
- 31 C. Tang, P. Georgopoulos, M. E. Fine, J. B. Cohen, M. Nygren, G. S. Knapp and A. Aldred, *Phys. Rev. B*, 1985, **31**, 1000.
- 32 L. Whittaker, T.-L. Wu, C. J. Patridge, G. Sambandamurthy and S. Banerjee, *J. Mater. Chem.*, 2011, **21**, 5580.
- 33 L. Whittaker, T.-L. Wu, A. Stabile, G. Sambandamurthy and S. Banerjee, *ACS Nano*, 2011, **5**, 8861.
- 34 M. C. Putnam, D. B. Turner-Evans, M. D. Kelzenberg, S. W. Boettcher, N. S. Lewis and H. A. Atwater, *Appl. Phys. Lett.*, 2009, **95**, 163116.
- 35 Y. Ahn, J. Dunning and J. Park, *Nano Lett.*, 2005, **5**, 1367.
- 36 R. Graham, C. Miller, E. Oh and D. Yu, *Nano Lett.*, 2011, **11**, 717.
- 37 Y. Gu, J. P. Romankiewicz, J. K. David, J. L. Lensch and L. J. Lauhon, *Nano Lett.*, 2006, **6**, 948.
- 38 J. E. Allen, E. R. Hemesath and L. J. Lauhon, *Nano Lett.*, 2009, **9**, 1903.
- 39 Y. H. Ahn, A. W. Tsen, B. Kim, Y. W. Park and J. Park, *Nano Lett.*, 2007, **7**, 3320.
- 40 Y.-J. Doh, K. N. Maher, L. Ouyang, C. L. Yu, H. Park and J. Park, *Nano Lett.*, 2008, **8**, 4552.
- 41 J. M. Atkin, S. Berweger, E. K. Chavez, M. B. Raschke, J. Cao, W. Fan and J. Wu, *Phys. Rev. B: Condens. Matter Mater. Phys.*, 2012, **85**, 020101.
- 42 D. B. McWhan, M. Marezio, J. P. Remeika and P. D. Dernier, *Phys. Rev. B: Solid State*, 1974, **10**, 490.
- 43 H. Kuzmany, *Solid State Spectroscopy*, Springer, New York, 1998.
- 44 C. Marini, E. Arcangeletti, D. Di Castro, L. Baldassare, A. Perucchi, S. Lupi, L. Malvasi, L. Boeri, E. Pomjakushina, K. Conder and P. Postorino, *Phys. Rev. B: Condens. Matter Mater. Phys.*, 2008, **77**, 235111.
- 45 J. Cao, Y. Gu, W. Fan, L. Q. Chen, D. F. Ogletree, K. Chen, N. Tamura, M. Kunz, C. Barrett, J. Seidel and J. Wu, *Nano Lett.*, 2010, **10**, 2667.
- 46 P. Schilbe, *Phys. B*, 2002, **316–317**, 600.
- 47 J. Y. Chou, J. L. Lensch-Falk, E. R. Hemesath and L. J. Lauhon, *J. Appl. Phys.*, 2009, **105**, 034310.
- 48 H. W. Liu, L. M. Wong, S. J. Wang, S. H. Tang and X. H. Zhang, *J. Phys.: Condens. Matter*, 2012, **24**, 415604.
- 49 M. Imada, A. Fujimori and Y. Tokura, *Rev. Mod. Phys.*, 1998, **70**, 1039.
- 50 K. Joondong, Y. Ju-Hyung, K. Chang Hyun, P. Yun Chang, W. Ju Yeon, P. Jeunghee, L. Jung-Ho, Y. Junsin and H. Chang-Soo, *Nanotechnology*, 2010, **21**, 115205.
- 51 A. Tselev, E. Strelcov, I. A. Luk'yanchuk, J. D. Budai, J. Z. Tischler, I. N. Ivanov, K. Jones, R. Proksch, S. V. Kalinin and A. Kolmakov, *Nano Lett.*, 2010, **10**, 2003.
- 52 S.-C. Kung, W. E. van der Veer, F. Yang, K. C. Donovan and R. M. Penner, *Nano Lett.*, 2010, **10**, 1481.
- 53 J.-J. Wang, F.-F. Cao, L. Jiang, Y.-G. Guo, W.-P. Hu and L.-J. Wan, *J. Am. Chem. Soc.*, 2009, **131**, 15602.
- 54 P. Wu, Y. Dai, Y. Ye, Y. Yin and L. Dai, *J. Mater. Chem.*, 2011, **21**, 2563.
- 55 K. S. Stevens, M. Kinniburgh and R. Beresford, *Appl. Phys. Lett.*, 1995, **66**, 3518.
- 56 R. H. Bube, *J. Appl. Phys.*, 1960, **31**, 1301.
- 57 T. Mueller, F. Xia and P. Avouris, *Nat. Photonics*, 2010, **4**, 297.
- 58 N. Mathews, B. Varghese, C. Sun, V. Thavasi, B. P. Andreasson, C. H. Sow, S. Ramakrishna and S. G. Mhaisalkar, *Nanoscale*, 2010, **2**, 1984.
- 59 S. Mathur, S. Barth, H. Shen, J.-C. Pyun and U. Werner, *Small*, 2005, **1**, 713.
- 60 X. Fang, L. Hu, K. Huo, B. Gao, L. Zhao, M. Liao, P. K. Chu, Y. Bando and D. Golberg, *Adv. Funct. Mater.*, 2011, **21**, 3907.
- 61 F. Xia, T. Mueller, Y.-m. Lin, A. Valdes-Garcia and P. Avouris, *Nat. Nanotechnol.*, 2009, **4**, 839.
- 62 J. Lu, C. Sun, M. Zheng, Y. Wang, M. Nripan, J. A. van Kan, S. G. Mhaisalkar and C. H. Sow, *J. Phys. Chem. C*, 2012, **116**, 22015.
- 63 A. Zhang, H. Kim, J. Cheng and Y.-H. Lo, *Nano Lett.*, 2010, **10**, 2117.
- 64 M. C. Hamilton, S. Martin and J. Kanicki, *IEEE Trans. Electron Devices*, 2004, **51**, 877.
- 65 C. Soci, D. Moses, Q.-H. Xu and A. J. Heeger, *Phys. Rev. B: Condens. Matter Mater. Phys.*, 2005, **72**, 245204.
- 66 C. Miller, M. Triplett, J. Lammatao, J. Suh, D. Fu, J. Wu and D. Yu, *Phys. Rev. B: Condens. Matter Mater. Phys.*, 2012, **85**, 085111.
- 67 M. Rini, Z. Hao, R. W. Schoenlein, C. Giannetti, F. Parmigiani, S. Fourmaux, J. C. Kieffer, A. Fujimori, M. Onoda, S. Wall and A. Cavalleri, *Appl. Phys. Lett.*, 2008, **92**, 181904.
- 68 C.-Y. Hsu, D.-H. Lien, S.-Y. Lu, C.-Y. Chen, C.-F. Kang, Y.-L. Chueh, W.-K. Hsu and J.-H. He, *ACS Nano*, 2012, **6**, 6687.